Ultra-compact silicon photonic devices reconfigured by an optically induced semiconductor-to-metal transition

Judson D. Ryckman,[1,*] Kent A. Hallman,[2] Robert E. Marvel,[2] Richard F. Haglund, Jr.,[2,3] and Sharon M. Weiss[1,2,3]

[1]*Department of Electrical Engineering and Computer Science, Vanderbilt University, Nashville, TN 37235, USA*
[2]*Department of Physics and Astronomy, Vanderbilt University, Nashville, TN 37235, USA*
[3]*Interdisciplinary Materials Science Program, Vanderbilt University, Nashville, TN 37234-0106, USA*
[*]*j.ryckman@vanderbilt.edu*

Abstract: Vanadium dioxide (VO_2) is a promising reconfigurable optical material and has long been a focus of condensed matter research owing to its distinctive semiconductor-to-metal phase transition (SMT), a feature that has stimulated recent development of thermally reconfigurable photonic, plasmonic, and metamaterial structures. Here, we integrate VO_2 onto silicon photonic devices and demonstrate all-optical switching and reconfiguration of ultra-compact broadband Si-VO_2 absorption modulators ($L < 1$ μm) and ring-resonators ($R \sim \lambda_0$). Optically inducing the SMT in a small, ~0.275 μm^2, active area of polycrystalline VO_2 enables Si-VO_2 structures to achieve record values of absorption modulation, ~4 dB μm^{-1}, and intracavity phase modulation, ~π/5 rad μm^{-1}. This in turn yields large, tunable changes to resonant wavelength, $|\Delta\lambda_{SMT}| \sim 3$ nm, approximately 60 times larger than Si-only control devices, and enables reconfigurable filtering and optical modulation in excess of 7 dB from modest Q-factor (~10^3), high-bandwidth ring resonators (>100 GHz). All-optical integrated Si-VO_2 devices thus constitute platforms for reconfigurable photonics, bringing new opportunities to realize dynamic on-chip networks and ultrafast optical shutters and modulators.

OCIS codes: (230.3120) Integrated optics devices; (160.6840) Thermo-optical materials; (230.5750) Resonators; (230.4110) Modulators; (130.4815) Optical switching devices.

References and Links

1. A. S. Liu, R. Jones, L. Liao, D. Samara-Rubio, D. Rubin, O. Cohen, R. Nicolaescu, and M. Paniccia, "A high-speed silicon optical modulator based on a metal-oxide-semiconductor capacitor," Nature **427**(6975), 615–618 (2004).
2. Q. F. Xu and M. Lipson, "All-optical logic based on silicon micro-ring resonators," Opt. Express **15**(3), 924–929 (2007).
3. Q. F. Xu, B. Schmidt, S. Pradhan, and M. Lipson, "Micrometre-scale silicon electro-optic modulator," Nature **435**(7040), 325–327 (2005).
4. M. Li, W. H. P. Pernice, C. Xiong, T. Baehr-Jones, M. Hochberg, and H. X. Tang, "Harnessing optical forces in integrated photonic circuits," Nature **456**(7221), 480–484 (2008).
5. P. B. Deotare, I. Bulu, I. W. Frank, Q. M. Quan, Y. N. Zhang, R. Ilic, and M. Loncar, "All optical reconfiguration of optomechanical filters," Nat Commun **3**, 846 (2012).
6. M. Bagheri, M. Poot, M. Li, W. P. H. Pernice, and H. X. Tang, "Dynamic manipulation of nanomechanical resonators in the high-amplitude regime and non-volatile mechanical memory operation," Nat. Nanotechnol. **6**(11), 726–732 (2011).
7. N. N. Feng, D. Z. Feng, S. R. Liao, X. Wang, P. Dong, H. Liang, C. C. Kung, W. Qian, J. Fong, R. Shafiiha, Y. Luo, J. Cunningham, A. V. Krishnamoorthy, and M. Asghari, "30GHz Ge electro-absorption modulator integrated with 3 μm silicon-on-insulator waveguide," Opt. Express **19**(8), 7062–7067 (2011).
8. M. Liu, X. Yin, E. Ulin-Avila, B. Geng, T. Zentgraf, L. Ju, F. Wang, and X. Zhang, "A graphene-based broadband optical modulator," Nature **474**(7349), 64–67 (2011).
9. J. Clark and G. Lanzani, "Organic photonics for communications," Nat. Photonics **4**(7), 438–446 (2010).

#187396 - $15.00 USD Received 19 Mar 2013; revised 21 Apr 2013; accepted 21 Apr 2013; published 25 Apr 2013

10. C. Koos, P. Vorreau, T. Vallaitis, P. Dumon, W. Bogaerts, R. Baets, B. Esembeson, I. Biaggio, T. Michinobu, F. Diederich, W. Freude, and J. Leuthold, "All-optical high-speed signal processing with silicon-organic hybrid slot waveguidesx," Nat. Photonics **3**(4), 216–219 (2009).
11. J. Leuthold, C. Koos, and W. Freude, "Nonlinear silicon photonics," Nat. Photonics **4**(8), 535–544 (2010).
12. J. Nag and R. F. Haglund, Jr., "Synthesis of vanadium dioxide thin films and nanoparticles," J. Phys. Condens. Matter **20**(26), 264016 (2008).
13. H. W. Verleur, A. S. Barker, and C. N. Berglund, "Optical Properties of VO_2 between 0.25 and 5 eV," Phys. Rev. **172**(3), 788–798 (1968).
14. J. Cao, E. Ertekin, V. Srinivasan, W. Fan, S. Huang, H. Zheng, J. W. L. Yim, D. R. Khanal, D. F. Ogletree, J. C. Grossman, and J. Wu, "Strain engineering and one-dimensional organization of metal-insulator domains in single-crystal vanadium dioxide beams," Nat. Nanotechnol. **4**(11), 732–737 (2009).
15. D. Ruzmetov, G. Gopalakrishnan, J. D. Deng, V. Narayanamurti, and S. Ramanathan, "Electrical triggering of metal-insulator transition in nanoscale vanadium oxide junctions," J. Appl. Phys. **106**(8), 083702 (2009).
16. M. Nakano, K. Shibuya, D. Okuyama, T. Hatano, S. Ono, M. Kawasaki, Y. Iwasa, and Y. Tokura, "Collective bulk carrier delocalization driven by electrostatic surface charge accumulation," Nature **487**(7408), 459–462 (2012).
17. M. Liu, H. Y. Hwang, H. Tao, A. C. Strikwerda, K. Fan, G. R. Keiser, A. J. Sternbach, K. G. West, S. Kittiwatanakul, J. Lu, S. A. Wolf, F. G. Omenetto, X. Zhang, K. A. Nelson, and R. D. Averitt, "Terahertz-field-induced insulator-to-metal transition in vanadium dioxide metamaterial," Nature **487**(7407), 345–348 (2012).
18. J. Wei, H. Ji, W. Guo, A. H. Nevidomskyy, and D. Natelson, "Hydrogen stabilization of metallic vanadium dioxide in single-crystal nanobeams," Nat. Nanotechnol. **7**(6), 357–362 (2012).
19. M. Hada, D. Zhang, A. Casandruc, R. J. D. Miller, Y. Hontani, J. Matsuo, R. E. Marvel, and R. F. Haglund, Jr., "Hot electron injection driven phase transitions," Phys. Rev. B **86**(13), 134101 (2012).
20. A. Cavalleri, C. Tóth, C. W. Siders, J. A. Squier, F. Ráksi, P. Forget, and J. C. Kieffer, "Femtosecond structural dynamics in VO_2 during an ultrafast solid-solid phase transition," Phys. Rev. Lett. **87**(23), 237401 (2001).
21. A. Cavalleri, T. Dekorsy, H. H. W. Chong, J. C. Kieffer, and R. W. Schoenlein, "Evidence for a structurally-driven insulator-to-metal transition in VO_2: A view from the ultrafast timescale," Phys. Rev. B **70**(16), 161102 (2004).
22. M. J. Dicken, K. Aydin, I. M. Pryce, L. A. Sweatlock, E. M. Boyd, S. Walavalkar, J. Ma, and H. A. Atwater, "Frequency tunable near-infrared metamaterials based on VO_2 phase transition," Opt. Express **17**(20), 18330–18339 (2009).
23. T. Driscoll, H.-T. Kim, B.-G. Chae, B.-J. Kim, Y.-W. Lee, N. M. Jokerst, S. Palit, D. R. Smith, M. Di Ventra, and D. N. Basov, "Memory Metamaterials," Science **325**(5947), 1518–1521 (2009).
24. M. Rini, A. Cavalleri, R. W. Schoenlein, R. López, L. C. Feldman, R. F. Haglund, Jr., L. A. Boatner, and T. E. Haynes, "Photoinduced phase transition in VO_2 nanocrystals: ultrafast control of surface-plasmon resonance," Opt. Lett. **30**(5), 558–560 (2005).
25. A. Joushaghani, B. A. Kruger, S. Paradis, D. Alain, J. S. Aitchison, and J. K. S. Poon, "Sub-volt broadband hybrid plasmonic-vanadium dioxide switches," Appl. Phys. Lett. **102**(6), 061101 (2013).
26. R. M. Briggs, I. M. Pryce, and H. A. Atwater, "Compact silicon photonic waveguide modulator based on the vanadium dioxide metal-insulator phase transition," Opt. Express **18**(11), 11192–11201 (2010).
27. J. D. Ryckman, V. Diez-Blanco, J. Nag, R. E. Marvel, B. K. Choi, R. F. Haglund, and S. M. Weiss, "Photothermal optical modulation of ultra-compact hybrid Si-VO_2 ring resonators," Opt. Express **20**(12), 13215–13225 (2012).
28. M. A. Kats, D. Sharma, J. Lin, P. Genevet, R. Blanchard, Z. Yang, M. M. Qazilbash, D. N. Basov, S. Ramanathan, and F. Capasso, "Ultra-thin perfect absorber employing a tunable phase change material," Appl. Phys. Lett. **101**(22), 221101 (2012).
29. J. M. Choi, R. K. Lee, and A. Yariv, "Control of critical coupling in a ring resonator-fiber configuration: application to wavelength-selective switching, modulation, amplification, and oscillation," Opt. Lett. **26**(16), 1236–1238 (2001).
30. M. Rini, Z. Hao, R. W. Schoenlein, C. Giannetti, F. Parmigiani, S. Fourmaux, J. C. Kieffer, A. Fujimori, M. Onoda, S. Wall, and A. Cavalleri, "Optical switching in VO_2 films by below-gap excitation," Appl. Phys. Lett. **92**(18), 181904 (2008).
31. R. E. Marvel, K. Appavoo, B. K. Choi, J. Nag, and R. F. Haglund, Jr., "Electron-beam deposition of vanadium dioxide thin films," Appl. Phys. A, 10.1007/s00339-012-7324-5 (2012).
32. C. Kübler, H. Ehrke, R. Huber, R. Lopez, A. Halabica, R. F. Haglund, Jr., and A. Leitenstorfer, "Coherent structural dynamics and electronic correlations during an ultrafast insulator-to-metal phase transition in VO_2," Phys. Rev. Lett. **99**(11), 116401 (2007).
33. S. Wall, D. Wegkamp, L. Foglia, K. Appavoo, J. Nag, R. F. Haglund, Jr., J. Stähler, and M. Wolf, "Ultrafast changes in lattice symmetry probed by coherent phonons," Nat Commun **3**, 721 (2012).
34. Z. S. Tao, T. R. T. Han, S. D. Mahanti, P. M. Duxbury, F. Yuan, C. Y. Ruan, K. Wang, and J. Q. Wu, "Decoupling of Structural and Electronic Phase Transitions in VO_2," Phys. Rev. Lett. **109**(16), 166406 (2012).
35. T. K. Liang, L. R. Nunes, T. Sakamoto, K. Sasagawa, T. Kawanishi, M. Tsuchiya, G. R. A. Priem, D. Van Thourhout, P. Dumon, R. Baets, and H. K. Tsang, "Ultrafast all-optical switching by cross-absorption modulation in silicon wire waveguides," Opt. Express **13**(19), 7298–7303 (2005).
36. M. M. Qazilbash, M. Brehm, B. G. Chae, P. C. Ho, G. O. Andreev, B. J. Kim, S. J. Yun, A. V. Balatsky, M. B. Maple, F. Keilmann, H. T. Kim, and D. N. Basov, "Mott transition in VO_2 revealed by infrared spectroscopy and nano-imaging," Science **318**(5857), 1750–1753 (2007).

#187396 - $15.00 USD Received 19 Mar 2013; revised 21 Apr 2013; accepted 21 Apr 2013; published 25 Apr 2013

37. S. Lysenko, A. Rua, V. Vikhnin, F. Fernandez, and H. Liu, "Insulator-to-metal phase transition and recovery processes in VO_2 thin films after femtosecond laser excitation," Phys. Rev. B **76**(3), 035104 (2007).
38. Y. Zhang and S. Ramanathan, "Analysis of "on" and "off" times for thermally driven VO_2 metal-insulator transition nanoscale switching devices," Solid-State Electron. **62**(1), 161–164 (2011).
39. A. Pashkin, C. Kübler, H. Ehrke, R. Lopez, A. Halabica, R. F. Haglund, R. Huber, and A. Leitenstorfer, "Ultrafast insulator-metal phase transition in VO_2 studied by multiterahertz spectroscopy," Phys. Rev. B **83**(19), 195120 (2011).
40. P. Dong, W. Qian, H. Liang, R. Shafiiha, D. Z. Feng, G. L. Li, J. E. Cunningham, A. V. Krishnamoorthy, and M. Asghari, "Thermally tunable silicon racetrack resonators with ultralow tuning power," Opt. Express **18**(19), 20298–20304 (2010).
41. R. Lopez, R. F. Haglund, L. C. Feldman, L. A. Boatner, and T. E. Haynes, "Optical nonlinearities in VO_2 nanoparticles and thin films," Appl. Phys. Lett. **85**(22), 5191–5193 (2004).
42. J. Nag, R. F. Haglund, E. Andrew Payzant, and K. L. More, "Non-congruence of thermally driven structural and electronic transitions in VO_2," J. Appl. Phys. **112**(10), 103532 (2012).
43. T. L. Cocker, L. V. Titova, S. Fourmaux, G. Holloway, H. C. Bandulet, D. Brassard, J. C. Kieffer, M. A. El Khakani, and F. A. Hegmann, "Phase diagram of the ultrafast photoinduced insulator-metal transition in vanadium dioxide," Phys. Rev. B **85**(15), 155120 (2012).
44. H. S. Rong, R. Jones, A. S. Liu, O. Cohen, D. Hak, A. Fang, and M. Paniccia, "A continuous-wave Raman silicon laser," Nature **433**(7027), 725–728 (2005).
45. J. D. Ryckman and S. M. Weiss, "Low mode volume slotted photonic crystal single nanobeam cavity," Appl. Phys. Lett. **101**(7), 071104 (2012).

1. Introduction

Active photonic devices featuring compact size and a large, rapid, and energy efficient optical response are essential to nanophotonic technologies incorporating reconfigurable filters, lasers, photonic networks, optical memories, and optical modulators. While silicon remains the preferred platform for large-scale manufacturing and provides natural advantages for optoelectronic integration, silicon suffers from limited dynamic optical functionality owing to its indirect band gap and modest electro-optic and nonlinear responses. Electro-optic or nonlinear effects in silicon can in fact be used in modulators or optical logic components, for example, but this typically requires long-path-length interferometers [1] (mm scale) or very narrow band resonators [2, 3] (less than 15 GHz), which are extremely sensitive to thermal or ambient fluctuations and fabrication errors.

Circumventing these challenges and realizing devices with improved functionality continues to be a central aim of nanophotonics research. One option is to construct active optical devices through optomechanics [4]. Utilizing the robust mechanical properties and large refractive index of silicon, it is possible to construct devices whose optical properties are exquisitely sensitive to mechanical actuation or reconfiguration. Although modest optomechanical response times (~μs) may limit their use in optical modulation, robust active devices capable of all-optical operation, ranging from reconfigurable filters [5] to optical memories [6], have been demonstrated. A second option is to harness the electro-optic or nonlinear properties of secondary materials integrated onto silicon, such as germanium, graphene, or organics. Electro-absorption effects in germanium [7] and graphene [8] have in fact been used to construct broadband optical modulators operating above GHz speeds; however, these devices are still tens of microns in length, and not suitable for on-demand optical routing, filtering, or all-optical switching. Silicon-organic hybrid geometries can provide all-optical and ultrafast operation capabilities [9, 10], but require very long (100 μm to several mm) interaction lengths even in waveguides with very high nonlinear waveguide parameters ($\gamma > 10^5$ W^{-1} km^{-1}) or slow-light effects [11].

The challenges highlighted by these examples motivate a continued search for alternative materials that can be integrated with silicon photonics to provide a large, rapid, and energy-efficient optical response while promoting wavelength-scale device dimensions and the capability for all-optical operation. Vanadium dioxide (VO_2) is a promising active optical material owing to its semiconductor-to-metal phase transition (SMT), which provides orders of magnitude change in resistivity, as well as large changes to absorption and refractive index [12]. The SMT alters the optical properties of VO_2 from the near- to far-infrared. The most substantial optical contrast between the semiconducting and metallic states occurs near 1.5 μm, making VO_2 particularly attractive for applications in optical communications [13]. The

#187396 - $15.00 USD Received 19 Mar 2013; revised 21 Apr 2013; accepted 21 Apr 2013; published 25 Apr 2013

first-order SMT is nearly congruent with a structural transition from a monoclinic to rutile crystal structure and occurs above a critical temperature T_c ~67 °C (340K). Importantly, it has been shown that the SMT of VO_2 can be triggered by strain [14], electric current or bias [15, 16], terahertz electric fields [17], hydrogenation [18], hot-electron injection [19], and all-optical pumping [20]. In the case of all-optical pumping, the transition has been shown to occur on timescales comparable to the pump pulse duration, down to ~75 fs [21]. The SMT is fully reversible and has recently been demonstrated at least in principle for use in a variety of reconfigurable or active metamaterial [22, 23], plasmonic [24, 25], and photonic [26–28] devices, generally relying on either global or local system heating.

Here we report the first demonstration of all-optical switching and reconfiguration of silicon photonic devices driven by a nanosecond photo-induced SMT in VO_2. Aside from triggering devices much faster than conventional thermal excitation, all-optical operation eliminates unwanted thermo-optic effects in the silicon waveguides, enabling large and robust reconfiguration. In the Si-VO_2 hybrid devices considered here, we demonstrate record values of optically induced broadband in-line absorption modulation (~4 dB μm^{-1}) and intracavity phase modulation (~π/5 rad μm^{-1}). By optically controlling attenuation or phase in both non-resonant and resonant structures, a variety of compact, highly reconfigurable and active photonic devices can be realized including filters, routers, shutters, and modulators. This work further sets the stage for SMT-driven optical limiters, semiconductor saturable absorbers, optical logic gates, and optical memories compatible with current silicon architectures.

2. Device and measurement geometries

Figures 1(a) and 1(b) illustrate the two device geometries utilized in this work. By integrating VO_2 onto single-mode silicon waveguides, the SMT can be harnessed to introduce a significant change in absorption, $\Delta\alpha$, as shown in Fig. 1(a). This non-resonant configuration utilizes the large contrast in the imaginary part of the VO_2 refractive index, $\Delta Im(n_{VO2}) = Im(n_M) - Im(n_S)$, on the order of + 2.6$i$ at 1550 nm [26]. The absorption induced in the waveguide can be engineered by controlling the evanescent field overlap with the VO_2 patch (*i.e.*, waveguide dimensions and patch thickness) and by tuning the VO_2 patch length. Because the absorption contrast provided by VO_2 exists throughout the near-infrared, device operation can be considered to be broadband; however, high optical contrast requires substantial volumes of VO_2 that may be detrimental to overall system performance.

Alternatively, the large contrast in the real part of the VO_2 refractive index, $\Delta Re(n_{VO2}) = Re(n_M) - Re(n_S)$, approximately −1.06 at 1550 nm, can be used to introduce a significant change in effective index or phase $\Delta\phi$. When incorporated into an optical cavity, such as an ultra-compact micro-ring resonator [R = 1.5 μm, Fig. 1(b)], a short ~0.5 μm-long patch is sufficient to promote large changes in resonant wavelength without significantly affecting Q-factor [22]. In principle, this configuration could serve as a wavelength-selective reconfigurable filter or modulator, or combined with a drop port for use as a router. With longer patch lengths, intracavity absorption modulation could also effectively extinguish resonances [29]; however, given the evident disadvantages of this approach in realistic device structures, in this work we will emphasize resonant frequency reconfiguration.

The pump-probe configuration used for these experiments is depicted in Fig. 1(c). Near infrared (NIR) lasers are used for both the cw probe (tunable from 1500 to 1600 nm) and pulsed pump (~25 ns FWHM, 1064 nm). Probe light is coupled into and out of the single-mode silicon-on-insulator (SOI) bus waveguides using compact on-chip tapers and lensed fibers, which are aligned using piezo-controlled XYZ stages. Pump light is focused onto the active Si-VO_2 devices at normal incidence through a 5x microscope objective. The spot size and pump fluence are estimated with an IR camera and power meter. Use of a large (~75 μm) radius spot size makes it easier to deliver low ~mJ/cm^2 pump fluences with precise control; these fluences correspond to ~pJ incident and sub-pJ absorbed energies for sub-micron-dimension VO_2 patches. Because the threshold fluence required to complete the SMT is

#187396 - $15.00 USD Received 19 Mar 2013; revised 21 Apr 2013; accepted 21 Apr 2013; published 25 Apr 2013

independent of pump-photon energy above the ~0.67 eV band gap of VO_2 [30], similar results would be expected for pumping at telecom frequencies (~0.8 eV). Probe optical transmission (typically of order ~μW) is monitored by a fast photo-detector and oscilloscope.

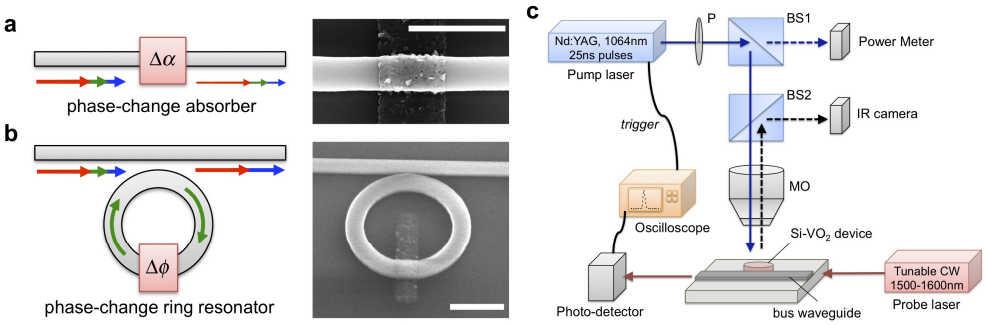

Fig. 1. Overview of the Si-VO_2 hybrid photonic devices and all-optical experimental setup. (a) Illustration of a phase-change absorber where the SMT induces a broadband change in absorption Δα. SEM image of a typical ultra-compact Si-VO_2 absorber with a 1 μm VO_2 patch length. (b) Illustration of a phase-change ring resonator where the SMT induces an intracavity phase modulation Δϕ. SEM image of an ultra-compact Si-VO_2 micro-ring resonator with radius R = 1.5 μm and a ~500 nm VO_2 patch length. Scale bars in both SEM images correspond to 1.5 μm, approximately the probe wavelength in free space. (c) Schematic of the experimental pump-probe configuration utilized in this work. Tunable probe laser transmission is monitored with a photo-detector and oscilloscope, while nanosecond-pulsed pump light is delivered to the device through a microscope objective (MO) and two beam-splitters (B1 and B2) with power controlled by a linear polarizer (P).

3. Methods

3.1 Device fabrication

The Si-VO_2 hybrid structures were made from silicon-on-insulator (SOI) wafers with a 220 nm p-type Si(100) device layer and a 1 μm buried oxide (SOITEC). Two stages of electron beam lithography (EBL) were used to pattern the silicon photonic structures and VO_2 patches. After the first stage of EBL (JEOL JBX-9300-100kV), the Si device layer was created by anisotropic reactive ion etching (Oxford PlasmaLab 100) with $C_4F_8/SF_6/Ar$ process gases. After the second stage of EBL (Raith eLine), amorphous sub-stoichiometric VO_x was deposited by electron-beam vaporization of V_2O_4 powder (100 mesh, 99.5% purity). Lift-off in acetone was performed prior to final annealing. The VO_x patches were annealed in a vacuum chamber under 250 mTorr of oxygen at 450 °C for ten minutes to form stoichiometric and polycrystalline VO_2 in accordance with our prior work [31]. This process temperature is thus within the regime required for CMOS-compatible processing ($T \leq 450$ °C).

3.2 All-optical experiments

Devices were tested in a pump-probe configuration as illustrated in Fig. 1(c). Probe light from a tunable cw laser (Santec TSL-510) was coupled into and out from ~mm length bus waveguides using polarization-maintaining lensed fibers (OZ Optics Ltd.) mounted on piezo-controlled XYZ stages. Photo-detection of the transmitted probe light was performed using a fiber-coupled avalanche photodiode photoreceiver (Newport 1647), with differential outputs monitored by an oscilloscope (Tektronix TDS 2024(c)). The oscilloscope was triggered directly from the nanosecond pump laser controller, a Q-switched Nd:YAG laser operating at 1064 nm with a low 10 Hz repetition rate (Continuum Minilite). Pump intensity was controlled by a polarizer (P) and delivered to the sample through two beamsplitters (BS1 and BS2) and a 5x, long working-distance microscope objective (MO). Use of a power meter

#187396 - $15.00 USD Received 19 Mar 2013; revised 21 Apr 2013; accepted 21 Apr 2013; published 25 Apr 2013

(Newport 2936 C) and IR camera (Sensors Unlimited 320M) enabled the calibration and measurement of pump fluence and precise positioning of the pump beam onto each device.

4. Pump-probe experiments

4.1 Si-VO_2 hybrid absorbers

Figure 2(a) shows the time-dependent optical transmission of the SOI waveguide with Si-VO_2 in-line absorbers for varying pump fluences (~0.5-8 mJ cm^{-2}) and patch lengths (L_{VO2} ~1 μm and 500 nm). Both devices exhibit an abrupt reduction in optical transmission in response to optical pumping. This drop occurs on a time-scale comparable to the pump-pulse FWHM (~25 ns), consistent with reports using ~10^{-8}-10^{-14} s laser pulses to optically trigger the SMT in VO_2 thin films [21]. In the devices tested here, the modulation depth increases approximately linearly with pump intensity and saturates near a threshold fluence of ~1.27 mJ/cm^2 [Fig. 4(a)]. This saturation is indicative of a completed SMT occurring throughout the VO_2 patch and is a hallmark of the structural phase transition (SPT) [32]. The observed threshold of ~1.27 mJ/cm^2 is comparable to other reports of the SMT spanning both nanosecond and femtosecond measurements [33, 34]. At threshold, based on the two device lengths measured, we estimate the modulation depth of the Si-VO_2 in-line absorbers to be 4 ± 0.3 dB μm^{-1}, which is approximately 40 times larger than monolayer graphene-on-Si absorbers (~0.1 dB μm^{-1}) [8] and more than three orders of magnitude larger than silicon-based two-photon cross-absorption modulation (~0.001 dB μm^{-1}) [35]. The insertion loss of the 1 μm Si-VO_2 device was within fiber-to-chip coupling variations, estimated between ~0.5-2 dB. Broadband device operation was verified over a wide range of probe wavelengths, 1500-1600nm, as shown in Fig. 2(c).

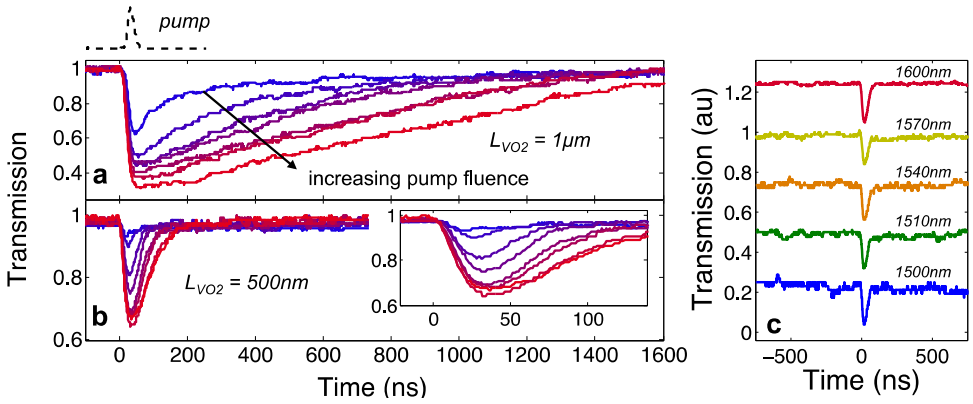

Fig. 2. Normalized probe transmission through Si-VO_2 absorbers with (a) 1 μm and (b) ~500 nm VO_2 patch lengths. The pump fluence is incrementally increased over the range ~0.5-8 mJ cm^{-2}. Inset shows a magnified view of the time response. The pump pulse is illustrated above and plotted on the same time scale. (c) Transmission through a 500 nm Si-VO_2 absorber for probe wavelengths ranging from 1500 to 1600 nm, demonstrating that the SMT of VO_2 can be used to realize broadband absorption modulation. Pump fluence was above threshold, ~5 mJ cm^{-2}. Plots are vertically stacked (0.25 offset) for clarity.

4.2 Si-VO_2 hybrid ring resonators

In addition to the Si-VO_2 in-line absorbers [Fig. 1(a)], we also tested the dynamic switching of Si-VO_2 hybrid micro-ring resonators [Fig. 1(b)]. Figure 3(a) shows the transmission spectra for an ultra-compact device, R = 1.5 μm, with an integrated ~500 nm long and ~70 nm thick VO_2 patch coating a portion of the ring waveguide. Owing primarily to bending losses at this ultra-compact ring radius, this device shows a modest Q ~10^3, resulting in an optical bandwidth exceeding 100 GHz. The time-dependent optical transmission for the

#187396 - $15.00 USD Received 19 Mar 2013; revised 21 Apr 2013; accepted 21 Apr 2013; published 25 Apr 2013

pump-probe experiment is shown in Fig. 3(b), where probe wavelength is tuned to match the resonance minimum (λ = 1588.5 nm). Photoinducing the SMT results in an abrupt increase in transmission, estimated in this case to be ~7.2 dB, followed by a slower relaxation to the low initial value. The observed modulation depth is several times larger than what can be achieved for the in-line absorber with the same active VO_2 area. The large increase in transmission observed for this modest Q-factor device suggests that the resonance wavelength is significantly modified by the photoinduced SMT. This is in stark contrast to conventional Si-only devices, where relatively weak electro-optic or nonlinear effects necessitate the use of high Q-factor, very narrow band (less than 5 GHz) resonators to observe significant modulation [3]. These effects are examined in greater detail in Section 5.

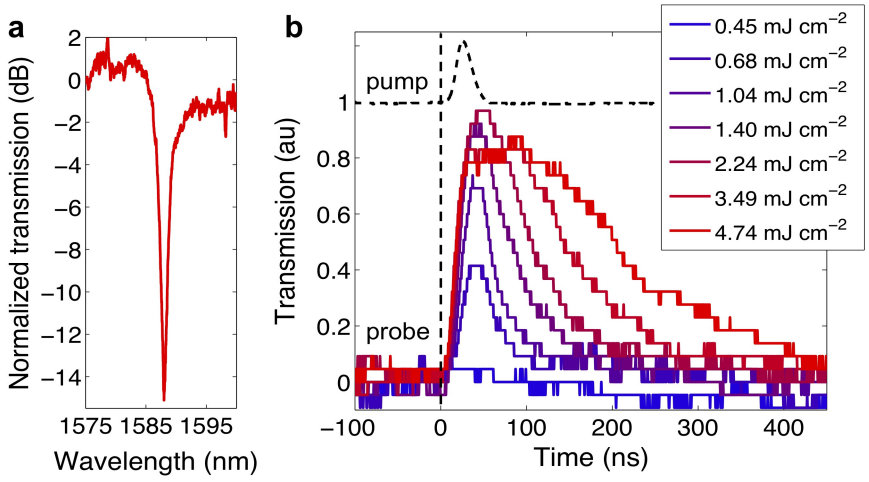

Fig. 3. (a) Typical resonance in the transmission spectra for a Si-VO_2 micro-ring resonator with radius R = 1.5μm. (b) Corresponding probe transmission where the probe wavelength is tuned to on-resonance (λ = 1588.5nm).

4.3 Relaxation time and dependence on VO_2 patch length

As shown in Fig. 3(a), the temporal dynamic of the reverse transition to the semiconducting phase of VO_2 can be significantly slower than the SMT, and depends strongly on both pump fluence and VO_2 patch length. The photoinduced SMT is an abrupt and potentially ultrafast athermal process, driven by photogeneration of electron-hole pairs and an electronically controlled lattice transformation into the higher-symmetry rutile structure [20, 33]. In our experiment, the ensuing thermalization transiently increases the internal temperature of the VO_2 patch [21]. Reversing the SPT is a thermally mediated relaxation process dependent on thermal diffusion and diffusion-limited nucleation of the monoclinic phase [32, 36]. It is important to emphasize that all-optical switching does not generate a localized heating effect, as the underlying silicon ring structure experiences virtually no temperature change during the SMT. Structural relaxation of the VO_2 patch depends strongly on the thermal interface to the underlying heat sink, in this case the Si waveguide. Because the Si waveguide remains at room temperature during the SMT, and has a much larger thermal conductivity than VO_2 (149 W m^{-1} K^{-1} *vs.* ~6.5 W m^{-1} K^{-1}), the transient thermal relaxation of the VO_2 patch to the semiconducting state can still be relatively fast (~10^{-9} s) [37, 38]. Dramatic improvements in relaxation time, $\tau_{M\text{-}S}$, to less than 10^{-12} s may be possible through various schemes, such as triggering the SMT without driving the SPT to completion [33, 39].

Our experiments show that in experiments where the SPT is driven to completion, simply changing the VO_2 patch length on a SOI waveguide to sub-micron dimensions, from 1 μm to 500 nm, reduces the relaxation decay time $\tau_{M\text{-}S}$ by approximately one order of magnitude

#187396 - $15.00 USD Received 19 Mar 2013; revised 21 Apr 2013; accepted 21 Apr 2013; published 25 Apr 2013

[Fig. 4(b)]. A thermal boundary-resistance model would predict a faster relaxation time when film thickness (d) is reduced ($\tau \propto d$) [37], but it cannot account for the observed effect when the VO_2 volume and thermal interface area are changed in the same proportion, as the classical relaxation time is $\tau \propto V/A$. This faster relaxation time with shorter VO_2 patches likely arises partially from the quasi-one-dimensional geometry of the SOI waveguide (for 1D, $\tau \propto L^2$ since the waveguide dimensions are comparable to the phonon mean free path in silicon, ~250 nm), or perhaps some other size-dependent effect in the nanocrystalline VO_2 patch. The Si-VO_2 hybrid ring resonators utilizing the shorter ~500 nm VO_2 patch length also show similarly reduced relaxation times, with some sample-to-sample variation [Fig. 4(b)]. We take this as further evidence that the thermal properties of the nanostructured interface play a significant role in the dynamics of the reverse SPT and can therefore be optimized.

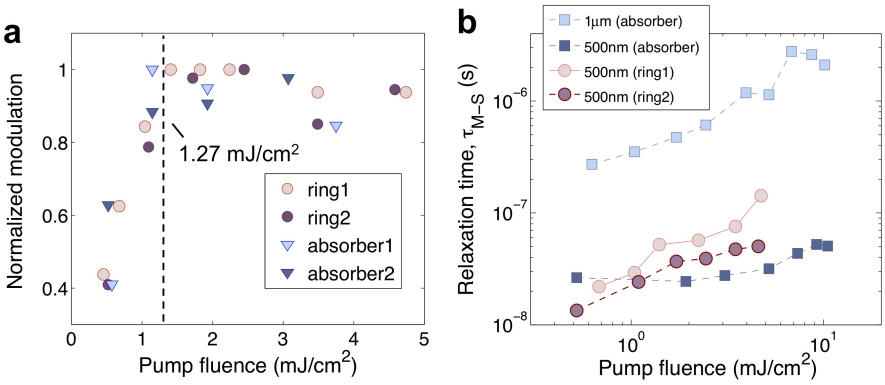

Fig. 4. (a) Saturation in the modulated probe signal is observed beyond a critical threshold fluence ~1.27 mJ cm^{-2}. (b) Relaxation time, τ_{M-S}, for the transition from the metallic state to the initial semiconducting state as a function of pump fluence plotted for Si-VO_2 absorbers and micro-ring resonators with 500 nm or 1 μm VO_2 patch lengths.

5. Si-VO_2 hybrid ring resonator spectral reconfiguration

5.1 Multi-wavelength pump-probe experiments

We carried out time-dependent measurements at varying probe wavelengths to examine the spectral characteristics of resonator response to the SMT. The response of an ultra-compact, R = 1.5 μm, Si-VO_2 hybrid ring resonator with L_{VO2} ~500 nm is shown in Fig. 5 and further analyzed in Fig. 6(a). This device is pumped at 1.9 mJ/cm^2, above the threshold required to complete the SMT by forming the rutile crystalline phase in VO_2. Optically triggering the SMT results in a rapid shift in resonant wavelength estimated to be $\Delta\lambda_{SMT} = -3.07$ nm [Fig. 6(a)], extracted by fitting the data to a Lorentzian lineshape. Performing this experiment on a control Si-only resonator, pumped at the same fluence, reveals a wavelength shift estimated to be $\Delta\lambda_{Si} = -0.057$ nm, nearly sixty times smaller [Fig. 5]. Whereas the large $\Delta\lambda_{SMT}$ reduction in resonant wavelength for the Si-VO_2 hybrid device arises from the substantial modification of the VO_2 refractive index, $\Delta Re(n_{VO2}) = -1.06$, the small $\Delta\lambda_{Si}$ reduction arises from the weak dependence of the silicon refractive index on free-carrier concentration, estimated in this case to change by $\Delta Re(n_{Si}) = -1.6 \times 10^{-4}$. The Si-only device was also tested under a pump fluence about six times higher, 11.5 mJ/cm^2, and showed a wavelength shift about six times larger than before, $\Delta\lambda_{Si} = -0.325$ nm [Fig. 5]. At this high fluence, in addition to the free-carrier effect, phonon excitations in the Si lattice produce a residual thermo-optic redshift as high as $\Delta\lambda_{Si} = +0.13$ nm, visible in Fig. 6(a) at times beyond ~30 ns. This corresponds to a transient temperature increase of the Si waveguide estimated between 1 and 2 °C [40]. No such effect is observed at 1.9 mJ/cm^2 fluence, indicating that the Si waveguide temperature is not affected by the pump pulse near but just above threshold. By eliminating the thermo-optic

#187396 - $15.00 USD Received 19 Mar 2013; revised 21 Apr 2013; accepted 21 Apr 2013; published 25 Apr 2013

contribution of the Si waveguide at the low pump fluence, the optical response of the device is entirely controlled by the SMT in the VO_2 patch. This greatly simplifies device operation and maximizes the achievable optical response, as the SMT in VO_2 and the thermo-optic effect in Si generally provide opposing contributions to refractive index. Furthermore, we can assume the timescale for device operation is dictated solely by the switching time of the VO_2.

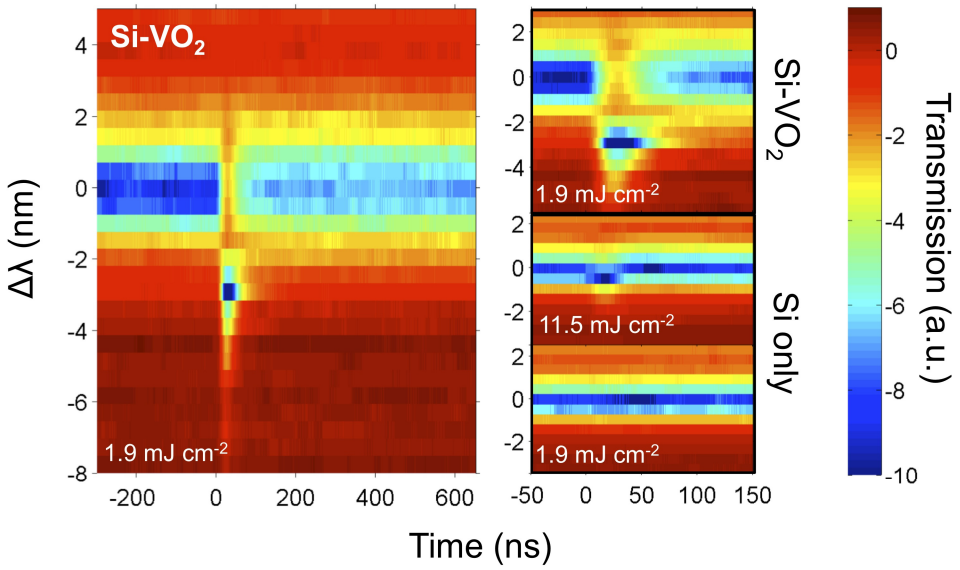

Fig. 5. Spectral reconfiguration of an ultra-compact Si-VO_2 micro-ring resonator. Mapped optical transmission for variable wavelength pump-probe measurements performed on a Si-VO_2 micro-ring resonator (R = 1.5 μm) at a pump fluence above threshold (1.9 mJ/cm^2). Right column reveals a zoomed in mapping for the same device as well as results from a Si-only control device pumped at 1.9 mJ/cm^2 and 11.5 mJ/cm^2. Colorbar indicates a logarithmic scale.

As shown in Fig. 6(a), the SMT-induced resonance shift and the SPT were completed in ~25-30 ns. At threshold, this time scale is primarily controlled by the FWHM of the pump pulse. Following optically driven reconfiguration of the resonator, the reverse SMT returns the VO_2 to its higher-index semiconducting state, bringing the resonant wavelength back to its initial value in ~50-70 ns. As mentioned earlier, this ~10^{-8} s relaxation time scale is not intrinsic to the phase-transition of VO_2 and can be controlled by a variety of factors including the thermal design, film dimensions, and method of triggering the SMT. Indeed based on the reported response times of VO_2 thin films optically excited with shorter pulses [20, 21, 41], it should be possible to extend device operation to ultrafast all-optical switching (less than a few ps). In the regime where the SMT coincides with a completed SPT from monoclinic to rutile structure, improving the timescale for the reverse transition could be achieved through more sophisticated thermal design, such as reducing the VO_2 thickness, depositing a top-cladding (e.g. SiO_2), or tailoring the SOI substrate geometry. Alternatively, recent THz conductivity experiments indicate lattice-relaxation times less than 2-3 ps are possible when the fluence for ultra-fast, ~15 fs, pump pulses is maintained below a threshold of 7 mJ/cm^2 [39]. In this regime, it has been hypothesized that photogenerated carriers may rapidly excite the electronic transition and rapidly decay through a fast trapping or relaxation pathways without cooperatively driving a complete SPT. There is additional evidence for the existence of a monoclinic metallic phase during both thermal and ultrafast excitation of VO_2 that suggests an operating window just above threshold where fast relaxation of a transient metallic phase is possible [36, 42, 43]. It may also be possible to enhance relaxation times using an applied bias to rapidly sweep out photogenerated carriers [44]. Thus there are several feasible design

#187396 - $15.00 USD Received 19 Mar 2013; revised 21 Apr 2013; accepted 21 Apr 2013; published 25 Apr 2013

strategies through which Si-VO_2 hybrids could be realized as a practical basis for ultrafast all-optical devices, such as modulators or logic gates, in silicon platforms.

The observed $\Delta\lambda_{SMT} = -3.07$nm for the ultra-compact, $R = 1.5$ µm, Si-VO_2 hybrid ring resonator corresponds to a resonant frequency reconfiguration of ~360 GHz. This large reconfiguration is achieved utilizing a very small ~0.275 µm^2 active area of ~70 nm thick VO_2, corresponding to a ~5.3% surface coverage on the micro-ring. By controlling the surface coverage, VO_2 thickness, or modal overlap, the resonant reconfiguration induced by the SMT could be tuned and optimized. For a hybrid Si-VO_2 waveguide, with Si dimensions 220 × 500 nm and a 70 nm thick VO_2 layer, the SMT is expected to produce a large change in effective index ΔN_{SMT} ~-0.14, as indicated by finite difference time domain (FDTD) modal calculations shown in Fig. 6(b). To demonstrate that the response derived from this effect is both large and highly tunable, we fabricated devices with the same ~0.275 µm^2 VO_2 patch area, but varying ring radii ranging from 1.5 to 10 µm. The maximum wavelength shift, $\Delta\lambda_{max}$, for each ring radius R was then determined by performing variable wavelength pump-probe measurements. As shown in Fig. 6(c), the magnitude of the resonant response, $|\Delta\lambda_{max}|$, follows an R^{-1} dependence. This agrees with calculations where the average effective index change in the ring resonator can be modeled as $\Delta N_{eff} = \Delta N_{SMT}\ L_{VO2}\ (2\pi R)^{-1}$. We experimentally estimate $\Delta N_{SMT} \sim -0.164 \pm 0.033$, from the relation $\Delta\lambda_{max}/\lambda_0 = \Delta N_{eff}/N_g$, where N_g is the group index of the ring waveguide (~4.4) and λ_0 is the initial resonant wavelength (~1550-1590 nm), which is close to, but slightly larger than, the value calculated in FDTD simulations. The intracavity phase modulation $\Delta\phi_{SMT} / L_{VO2} = 2\pi/\lambda_0\ \Delta N_{SMT}$ induced by the SMT is then estimated at ~π/5 rad µm^{-1}, while that of the Si-only device is estimated to be three orders of magnitude lower, ~π/5000 rad µm^{-1}. It is for this reason that the small (~0.275 µm^2) active area of VO_2, equivalent to ~5.3% surface coverage on the ring, can still provide a resonant response approximately sixty times larger than that of the Si-only device.

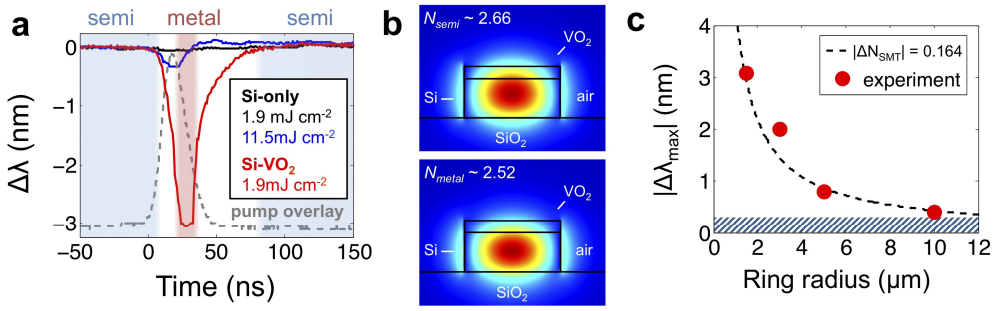

Fig. 6. Analysis of Si-VO_2 micro-ring resonator reconfiguration. (a) Resonant wavelength as a function of time, extracted from the variable wavelength pump-probe measurements shown in Fig. 5. The pump signal is overlaid for comparison purposes. (b) FDTD mode simulation for a hybrid Si-VO_2 waveguide, with Si dimensions 220 × 500 nm and a 70 nm thick VO_2 patch on top. (c) Magnitude of the resonance wavelength blue-shift $\Delta\lambda_{max}$, occurring in response to photo-inducing the SMT on Si-VO_2 micro-ring resonators with varying ring radii and a fixed ~500 nm VO_2 patch length. Shaded region indicates the regime where $\Delta\lambda < 0.3$ nm, corresponding to typical thermo-optic variability of Si resonators under temperature variations ± 3°C, also equivalent to ~2 linewidths for a high Q (~10^4) resonator.

5.2 Discussion

A notable advantage of a large resonant response is that devices can operate outside the regime where ambient effects, such as thermal fluctuations, can play a significant role. The shaded gray region in Fig. 6(c) covers the region where $\Delta\lambda \leq 0.3$ nm, and corresponds to a temperature tolerance of ± 3 °C for silicon resonators with a typical thermo-optic sensitivity

#187396 - $15.00 USD Received 19 Mar 2013; revised 21 Apr 2013; accepted 21 Apr 2013; published 25 Apr 2013

of ~0.1 nm/°C. This region also corresponds to roughly two linewidths for a cavity with Q ~10^4. High-Q silicon photonic devices that operate in this regime are highly susceptible to noise or error and thus require added complexity or energy consumption for active thermal compensation. The longer cavity lifetime of these high-Q resonators also limits the speed at which they can operate. Thus, constructing ultrafast reconfigurable photonic devices, capable of speeds exceeding 100 GHz, will ultimately require either non-resonant effects (e.g. interferometers, absorbers), or modest $Q \leq 10^3$ resonators with a large optical response. As noted previously [27], reducing the ring radius from 10 μm to 1.5 μm can reduce the Q-factor from ~10^4 to ~10^3 owing to increased bending losses. By providing larger enhancements for larger fractional VO_2 surface coverage, the Si-VO_2 platform further favors ultra-compact device geometries. This can be clearly seen in Fig. 6(c), where the smallest micro-ring resonator exhibits the largest resonant response. Given the fixed VO_2 volume, this is equivalent to a wavelength sensitivity inversely related to the cavity mode volume, V. While the $R = 1.5$ μm micro-ring has a low mode volume, ~$11.5(\lambda/n)^3$, further reducing the cavity mode volume would be attractive for realizing super-ultra-compact, ultra-low-power devices. For example, by integrating VO_2 with a slotted nanobeam cavity [45], where V is on the order of ~$0.01(\lambda/n)^3$, we anticipate that the same ~nm scale $\Delta\lambda$ resonant reconfiguration could be achieved at sub-femtoJoule switching energies using single nanoparticles of VO_2.

6. Conclusion

In summary, we have demonstrated all-optical operation of Si-VO_2 broadband in-line absorbers and micro-ring resonators. The laser-induced SMT in VO_2 yielded record values of modulation (~4 dB μm^{-1}) and intracavity phase modulation (~$\pi/5$ rad μm^{-1}) for all-optical silicon photonic devices. For resonant devices, the large optical response enables larger bandwidth, reduced ambient sensitivity, ultra-compact geometries, and reduced power requirements. With this platform, a wide variety of reconfigurable active photonic devices operating on the nanosecond time scale can be reduced to practice, including filters, routers, shutters, and modulators. Given the potential to trigger the SMT in less than 100 fs both optically and electro-optically, and with a plausible strategy for reducing the switch-off time below 3 ps, the Si-VO_2 platform could lead to a new class of ultrafast silicon photonic devices ranging from optical limiters to optical logic gates and ultrafast optical memories.

Acknowledgments

This work was supported in part by the Air Force Office of Scientific Research under Grant FA9550-10-1-0366 (G. Pomrenke). A portion of this research was conducted at the Center for Nanophase Materials Sciences, which is sponsored at Oak Ridge National Laboratory by the Scientific User Facilities Division, Office of Basic Energy Sciences, U.S. Department of Energy. Portions of this work were also performed at the Vanderbilt Institute of Nanoscale Science and Engineering, using facilities renovated under NSF ARI-R2 DMR-0963361. The authors wish to thank I. Kravchenko, S. Retterer, D. Hensley, and D. Briggs for their guidance at CNMS, and S. Avanesyan for assistance with the nanosecond laser. R.E.M. was supported by a research assistantship provided by a grant from the National Science Foundation (DMR-1207507). J.D.R. acknowledges support from a NSF Graduate Research Fellowship.